Acta Biomaterialia 56 (2017) 36–43

Contents lists available at ScienceDirect

Acta Biomaterialia

journal homepage: www.elsevier.com/locate/actabiomat

Full length article

Indentation across interfaces between stiff and compliant tissues ☆

Oliver E. Armitage, Michelle L. Oyen *

Cambridge University Engineering Dept, The Nanoscience Centre, 11 JJ Thomson Avenue, Cambridge CB3 0FF, UK

ARTICLE INFO

Article history:
Received 15 August 2016
Received in revised form 28 November 2016
Accepted 16 December 2016
Available online 4 January 2017

Keywords:
Nanoindentation
Finite element
Enthesis
Elastic modulus

ABSTRACT

Bone–tendon, bone–ligament and bone–cartilage junctions are multi-tissue interfaces that connect materials that differ by two orders of magnitude in mechanical properties, via gradual variations in mineral content and matrix composition. These sites mediate load transfer between highly dissimilar materials and are consequently a primary site of injury during orthopedic failure. Given the large incidence rate and the lack of suitable surgical solutions for their regeneration or repair, characterization of their natural structure and subsequent replication through tissue engineering is important. Here, we evaluate the ability and accuracy of instrumented indentation to characterize the mechanical properties of both biological tissues and engineered scaffolds with interfaces between materials that contain significant changes in mechanical properties. In this study, finite element simulations and reference samples are developed that characterize how accurately indentation measures the modulus of a material as it varies with distance across a continuous interface between dissimilar tissues with multiple orders of magnitude difference in properties. Finite element simulations accurately predicted discrepancies between the modulus function across an interface observed by indentation and the true modulus function of the material and hence allow us to understand the limits of instrumented indentation as a technique for quantifying gradual changes in material properties. It was found that in order to accurately investigate mechanical property variations in tissues with significant modulus heterogeneity the indenter size should be less than 10 percent of the expected length scale of the modulus variations.

Statement of Significance

The interfaces between stiff and compliant orthopedic tissues such as bone–tendon, bone–ligament and bone–cartilage are frequent sites of failure during both acute and chronic orthopedic injury and as such their replication via tissue engineering is of importance. The characterization and understanding of these tissue interfaces on a mechanical basis is a key component of elucidating the structure-function relationships that allow them to function naturally and hence a core component of efforts to replicate them. This work uses finite element models and exeperiments to outline the ability of instrumented indentation to characterize the elastic modulus variations across tissue interfaces and provides guidelines for investigators seeking to use this method to understand any interface between dissimilar tissues.

1. Introduction

Connective tissues in the musculoskeletal system are subdivided into tendons (bone–muscle interactions in tension), ligaments (bone–bone interactions in tension) and cartilage (bone–bone interactions in compression). These interfaces are a primary site of injury in the musculoskeletal system. In the US alone there are 600,000 rotator cuff tendon surgeries [1], 100,000 anterior cruciate ligament reconstructions [2] and 580,000 surgeries relating to osteoarthritis of the hip per year [3]. Yet, the bulk of current orthopedic tissue engineering efforts have focused on the repair of single homogeneous tissues such as bone [4] or tendon [5]. A small number of authors however, have focussed on the regeneration of the graded interface between bone and cartilage [6–9], or bone and ligaments or tendons [10,11]. Successful replication of the interfaces between different musculoskeletal tissues is essential for restoring proper joint function after injury, as merely juxtaposing ligament and bone during surgery does not result in regeneration of the natural multi-tissue interface [12–14]. In order to satisfactorily replace either the bone–tendon, bone–ligament or bone–cartilage interface after injury, graded tissue engineering scaffolds that

☆ Part of the Gradients in Biomaterials Special Issue, edited by Professors Brendan Harley and Helen Lu.

* Corresponding author.
E-mail address: mlo29@eng.cam.ac.uk (M.L. Oyen).

http://dx.doi.org/10.1016/j.actbio.2016.12.036
1742-7061/

properly mimic natural interface mechanical properties, will be required (*e.g.* [6–9,11,15–17]). Tissue engineering scaffolds must mimic the natural mechanical properties on both a macroscale to replace function [18,19], and on a microscale to control cell differentiation [20,21]. A prerequisite for a successful replication of these interfaces is a thorough understanding of the chemical and mechanical variations across the natural structure; the study of the mechanical component of this through indentation is the focus of the work contained herein.

Nanoindentation has been widely used to map the elastic modulus of heterogeneous materials [22] including natural materials such as teeth [23], cephalopod beaks [24] and coccinellidae feet [25], or engineering materials such as ceramic composites [26], metal grains [27] and thin film inclusions [28]. These studies frequently test stiff synthetic materials or stiff natural tissues with elastic moduli in the GPa range, as this is the optimal operating region of the majority of commercial nanoindentation instrumentation [29]. For example, Gupta et al. used nanoindentation to measure modulus across a tissue interface, the patella-cartilage osteochondral junction [30]; the tissue was dehydrated prior to testing, bringing the modulus into the optimal range of the instrumented indentation and reducing viscoelasticity [31,32]. The region over which elastic modulus and mineral content changed from the stiff to compliant tissue was found to be approximately 30μm wide. Abraham and Hauch [33,34] used nanoindentation to determine the change in elastic modulus through the insertional zones of human meniscal cartilage on hydrated samples using a spherical tip. In both studies, the transition region was found to be 200–400μm wide, similar to the width of the total tissue transition from tendon to bone through unmineralized and mineralized fibrocartilage; while being the width of the histological tissue transition this is not necessarily the width of the mechanical transition. The ability of instrumented indentation to be used as a tool to quantify small-scale variations in material properties depends on two characteristic lengths scales, the diameter, d, of the contact area between indenter and sample, and the width, W, over which significant changes in elastic properties occur across the sample. The contact patch diameter, d, is related to the indenter radius, R, via the indentation depth, h:

$$d = 2\sqrt{hR} \tag{1}$$

where d/W will be used to define the limits of the ability of instrumented indentation to map mechanical properties across elastic modulus gradients between stiff and compliant materials.

Hydrated biological tissues, which are generally more compliant than engineering materials, practically require large indenter tips in order to generate sufficient force on the test equipment in the range of displacements available in commercially available indenters [29]. As a consequence, the size of the contact patch between indenter and sample increases and a larger volume of material is deformed during a single indent. This reduces the spatial resolution of a modulus map across a sample, as the sampling volume of each indent is increased and hence a larger distance is required between successive indents for them to remain independent. As a consequence, transitions between stiff and compliant tissues can appear wider than their true size due to feature blurring introduced by measurement via indentation mapping. In order to demonstrate and quantify this effect, a finite element (FE) model of a line of indents across an interface between stiff and compliant materials is developed. This model is used to show how the function of modulus that is observed, $E_O(x)$, can be different from the true modulus function, $E_T(x)$, of the material, where x is the perpendicular distance from the interface. The difference between true and observed modulus functions is investigated as a function of the width of the true transition in modulus in the sample and the relative size of the indenter contact patch, defined by d/W. Experimental indentation data from a selection of interface samples is used to validate the results of the model. Finally, the FE model is used to analyze literature examples of indentation across biological interfaces and the implications for future studies are discussed.

2. Methods

2.1. Finite element model

A two-dimensional, linear, finite element model of an elastic solid in contact with a spherical indenter was constructed and meshed using ABAQUS 6.11 (Simula, Providence, RI, USA). The solid was modeled as having a gradient in elastic modulus that varied in the transverse direction with a sigmoid shaped logistic function to simulate a continuous interface between two dissimilar materials. The spherical indenter was modeled as a rigid body with one millimeter radius which contacted an elastic solid half space 40 mm wide by 20 mm tall at its top centre (Fig. 1). A refinement study of the width and height of the elastic solid showed that both were sufficiently large compared to indenter radius and indentation depth, respectively, to allow the results to be considered free of edge effects. The elastic solid was rigidly fixed at the base plane with an encastre boundary condition and unconstrained on the top and sides. The simulated indentation depth was chosen to control the characteristic indentation strain, ϵ, [35] where:

$$\epsilon \approx 0.2(h/R)^{1/2} \tag{2}$$

The simulated indentation depth was 0.0625mm, giving a characteristic indentation strain of 5%.

The elastic solid had a continuous quad mesh biased towards the contact point of the indenter. Directly under the contact patch in a 5 mm × 5 mm region the mesh elements were 0.01 mm × 0.01 mm and at the far edges of the sample, the elements were 0.5 mm 0.01 0.5 mm. A mesh refinement study in which the entire solid was meshed with uniform sized elements 0.01 mm square demonstrated that the mesh used for the study did not differ by more than 1% from the solution obtained with the finer, uniform mesh.

The elastic solid had a Poisson's ratio of $\nu = 0.4$, comparable to that of orthopedic biological tissues such as cartilage and bone [36,37]. A range of Poisson's ratio's from $\nu = 0.3$ to $\nu = 0.49$ were also tested in simulation and did not show a significant effect on the results. The transition in elastic modulus across the interface

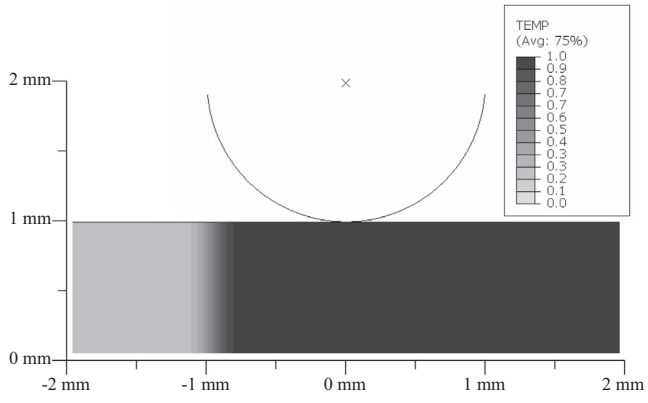

Fig. 1. A typical temperature field in the sample used to induce an elastic modulus field. The light to dark greyscale transition across the sample signifies the temperature change from 0 → 1. The modulus sigmoid in this figure is centered −1 mm from the indentation location.

was implemented through the use of a material with a temperature dependent elastic modulus. The temperature variation, $T(x)$, was generated via a sigmoid shaped logistic function:

$$T(x) = \frac{1}{1 + e^{-ax}} \tag{3}$$

resulting in a variation of the temperature from $0 \rightarrow 1$ with the shape shown in Fig. 2. Here, a, is a dimensionless number that controls the width of the transition region. The width of the function, W, is considered as the middle 90% of the transition *i.e.* the width between the 5% height, x_5, and the 95% height, x_{95}, where $T_i = T(x)|_{x=i}$:

$$x_i = \frac{1}{a} \ln\left(\frac{T_i}{1 - T_i}\right) \tag{4}$$

The width of the transition region is then:

$$W = 2 * \frac{1}{a} \ln\left(\frac{95}{5}\right) \approx \frac{5.89}{a} \text{ mm} \tag{5}$$

Fig. 2 shows two versions of $T(x)$ with different widths. The computational model linearly relates the elastic modulus of each mesh element to the temperature field by specification of the stiff modulus, E_S, at $T = 1$ and the compliant modulus, E_C at $T = 0$. In this way the true transition in modulus, $E_T(x)$, is implemented where the width can be controlled by setting a. Fig. 1 shows a simulation where the light to dark transition encodes the change in temperature (and hence elastic modulus) for a transition centered -1mm from the center of the indentation.

In order to simulate a line of indentation experiments across the interface, the center of the sigmoid transition in modulus was moved relative to the indenter contact patch for successive simulations. This was achieved with a recursive Python script that moved the center of the sigmoid for successive simulations and calculated the observed modulus via hertzian contact:

$$E = \frac{3P(1 - \nu^2)}{4R^{1/2}h^{3/2}} \tag{6}$$

The modulus at each point was calculated to give $E_O(x)$, the function of modulus observed through indentation. This could then be compared to $E_T(x)$, the true function of modulus through the sample.

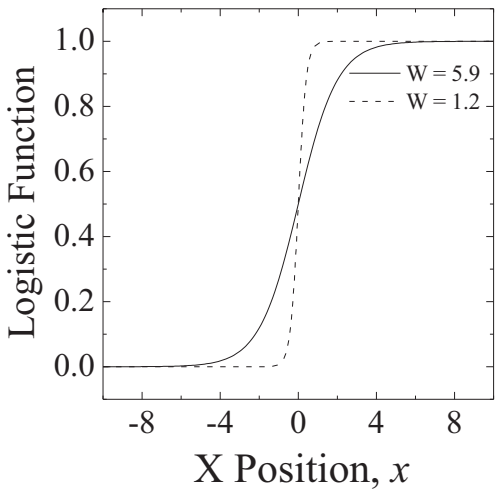

Fig. 2. A plot of the sigmoid shaped logistic function (Eq. (3)) used to generate a temperature field across x within the material, giving rise to a gradient in elastic modulus. This graph shows two transitions in modulus with different widths as defined in Eq. (5).

2.2. Materials

2.2.1. PDMS-nickel composites

A material containing an interface between stiff and compliant regions was synthesized by embedding an open cell nickel foam into half of a 10:1 PDMS block, Sylgard® 184 (Dow Corning, UK). Open cell Inconel nickel foam with a pore size in the range 200–300μm was obtained in 1.9mm thick sheets and cut into 2cm × 2cm sections. Vacuum cycling ensured complete backfilling of the foam with PDMS before curing, this gave a flat sheet of PDMS where one half contained an embedded open cell nickel foam.

2.2.2. Two phase gelatin gels

Gelatin gels were synthesized as an additional model interface. Large molecular weight (250 g bloom) gelatin, Sigma–Aldrich (UK), was cast into 7.5 wt% and 20 wt% gels, where 20 wt% gels were colored with a small amount of green food coloring for visualization. An interface gel was created by first setting the 20 wt% gel for 1 h in one half of a divided mold. After setting for 1 h the divider was removed and the 7.5 wt% gel solution was poured into the second half of the mold adjacent to the 20 wt% gel. Because the 20 wt% gel had not yet fully set, the latent heat of the 7.5 wt% gel allowed a distinct but mechanically joined interface to form across the boundary.

2.2.3. Partially demineralized bone

Four centimeter long sections of porcine scapula where partially demineralized via semi-submersion in a 0.01 M, pH 2, HCl solution. The bone sections were suspended into a beaker of HCl such that half the bone was submerged. After 36 h, the bone was removed and rinsed thoroughly in distilled water to remove the acid. This process resulted in a continuous piece of bone tissue, unchanged at one end and significantly reduced in mineral content—and hence stiffness—at the other end. Sections of partially demineralized porcine bone were then set in Acri-Kleer cold mounting epoxy (MetPrep, UK) and polished down to a 2.5 μm grit to form a flat surface for indentation.

2.3. Mechanical testing

Instrumented microindentation was performed on an Instron 5544 universal testing frame (Canton, MA, USA) using a 5 N load cell. Indentation was performed in displacement control with a ramp-hold loading profile; the displacement, h, is ramped at a constant rate to a fixed displacement, h_{max}. The load, P, displacement, h, and time, t, are recorded during testing. Testing parameters for each sample type can be seen in Table 1. Three samples of each type were used for testing and plots of modulus against distance from interface were generated from a regular grid of indents across the surface of the sample. Indents were placed in grid on the surface of the sample using a calibrated XY stage (LT6820, Kliendiek Nanotechnik, Reutlingen, DE). Indents in the PDMS-nickel composites were conducted using a 1.8 mm radius spherical indenter tip with $h_{max} = 0.1125$ mm, giving a contact diameter $d = 0.9$ mm and characteristic indentation strain $\epsilon = 5\%$. Indents in the PDMS-nickel sample were spaced 0.5 mm apart within 3 mm of the interface and 1 mm apart when further from the interface. Indents across the two phase gelatin gels were conducted using a 4.8 mm radius spherical indenter tip with $h_{max} = 1.5$ mm, giving a contact diameter $d = 5.3$ mm and characteristic indentation strain $\epsilon = 10\%$. Indents in the gelatin gels were arranged in a 5mm × 5mm grid angled at 15° to the interface, resulting in a range of distances from the interface at a higher resolution than a 5 mm grid oriented perpendicularly. Indents across the deminer-

Table 1
Table of indentation testing parameters for different samples. Indentation strain is calculated using Eq. (2).

	Technical replicates, n	Indenter radius, R (mm)	Indentation depth, h (mm)	Characteristic indentation strain, ε (%)
PDMS-nickel composites	3	1.8	0.1	4.5
Two phase gelatin gels	4	4.7	1.5	11.2
Demineralised bone	3	1.8	0.1	4.5

alized bone were conducted with the same indenter tip, indentation depth, contact diameter, indentation strain and grid spacing as for the PDMS-nickel composites.

3. Results

3.1. Finite element models

Finite element models were used to investigate the relationship between $E_T(x)$ and $E_O(x)$ for indents in the elastic modulus range relevant to indentation of biological stiff-compliant tissue interfaces. The observed width of the transition region, W_O, significantly exceed the true width of the transition region, W_T, if the length scale of indentation is larger than, or comparable to, that of the true modulus transition *i.e.* $d/W \geqslant 1$. In the extreme case of a perfectly sharp transition, the observed modulus function will still appear as a gradient (Fig. 3). For Fig. 3, $W_T = 0.45$mm, whereas the observed width is $W_O = 8.22$ mm, which is approximately twenty times the true width and ten times the contact diameter.

Varying d/W_T, the width, W_T, of the true modulus function relative to the contact diameter, d, and observing W_O, demonstrates that if the width of the true transition is much smaller than the contact diameter, any changes in $E_O(x)$ and W_O are almost indistinguishable (Fig. 4). Specifically the width W_O of $E_O(x)$ is not representative of the true width W_T of modulus transition in the sample when the length scale of indentation, d, is similar to or larger than true width W_T. Any changes observed in W_O in this case are likely within the experimental error of any experimental data. Further, this model demonstrates that to measure $E_T(x)$ within 90% accuracy the contact patch should be one tenth of the true modulus transition, $d/W \leqslant 0.1$.

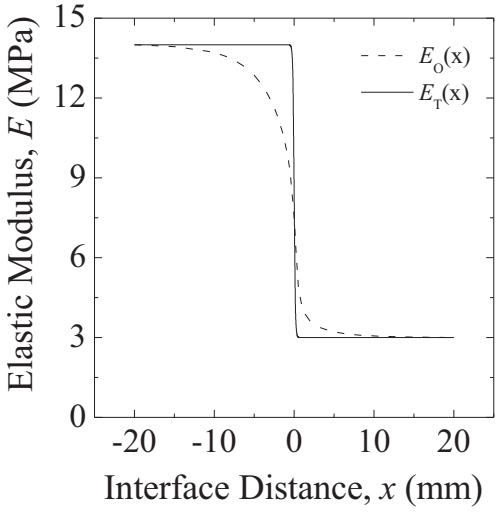

Fig. 3. A plot of observed elastic modulus, $E_O(x)$, and the true modulus, $E_T(x)$, vs distance from the interface for a finite element simulation of indentation across a change in modulus similar to that of the PDMS-nickel composites. The 95% width of the true transition region in $E_T(x)$, is $W_T = 0.45$ mm whereas the width of the observed transition region is $W_O = 8.22$ mm by simulated indentation. The stiff and compliant elastic moduli for this simulation were $E_S = 14$ MPa and $E_C = 3$ MPa.

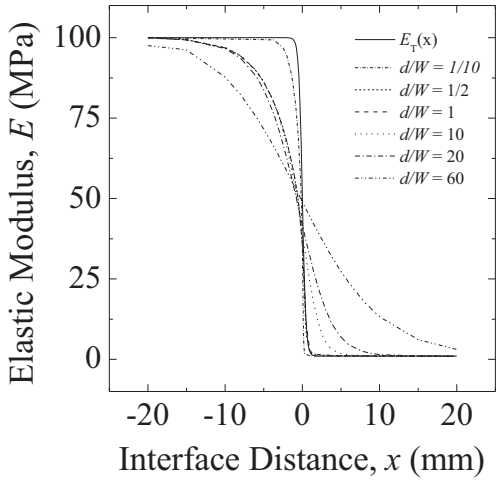

Fig. 4. A plot of observed elastic modulus vs distance from the interface for different ratio's of the interface width to contact patch diameter, d/W. This shows the changes in observed modulus function $E_O(x)$ obtained for $d/W = 1/10,\ 1/2,\ 1,\ 10,\ 20$ and 60. In this set of simulations the contact diameter was held constant and the interface width of the sample changed. Elastic moduli for this simulation were $E_S = 100$ MPa and $E_C = 1$ MPa.

The ratio between the stiff modulus, E_S, and compliant modulus, E_C, was also examined. Fig. 5 shows the comparison of two indentation simulations with different ratios of E_S/E_C. To allow graphical comparison of different plots these plots were normalized to the range $0 \rightarrow 1$ by $(E_O(x) - E_C)/E_S$. In Fig. 5 it can be seen that for samples with a greater modulus mismatch between the two sides of the interface the observed transition is sharper on the stiffer side and rounded off on the compliant side.

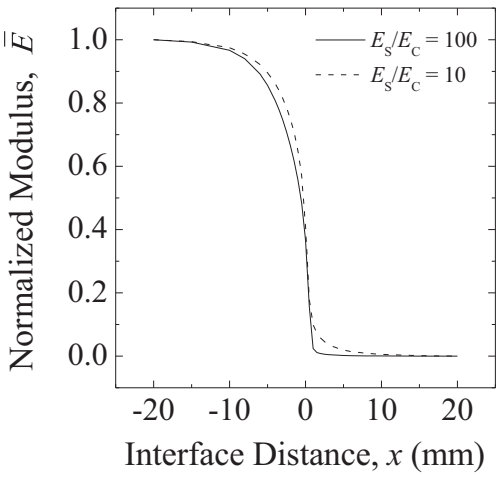

Fig. 5. A plot of simulated observed elastic modulus vs distance from the interface for different ratios of E_S/E_C. In this case both simulated observed modulus functions have been normalized to the range $0 \rightarrow 1$ to show how the non-symmetric sigmoid that is obtained as the observed modulus function is dependent on the ratio of upper to lower modulus. Functions were normalized by $(E_O(x) - E_L)/E_U$.

3.2. Experimental interface indentation

Experimental samples containing transitions in elastic modulus from stiff to compliant were used to validate the model by comparison of indentation maps across the interface with simulated data of the sample. In each case the observed width of the elastic modulus function, W_O, is recorded and compared to the true width, W_T, and the contact diameter, d.

3.2.1. PDMS-nickel composites

The observed gradient in modulus between the stiff and compliant sides of the PDMS-nickel composite sample is $W_O = 3$mm (Fig. 6). This is three times bigger than the contact patch of indentation $d = 0.9$ mm and twelve times bigger than the true modulus gradient between the two materials, $W_T = 250$ μm. The true gradient in modulus is assumed to occur over the width of a broken single foam cell at the edge of the nickel foam which is 250 μm wide. Simulation of the indentation mapping experiment with stiff and compliant side elastic moduli of $E_S = 19$ MPa and $E_C = 3$ MPa respectively, contact diameter and true modulus transition of $d = 0.9$ mm and $W_T = 250$μm. The model accurately predicted the shape of $E_O(x)$ and over predicted the observed width of the transition W_O to be 11 mm.

3.2.2. Two phase gelatin gels

The observed gradient in modulus for this sample is $W_O = 14.7$ mm (Fig. 7), three times greater than the contact diameter of the indent, $d = 5.3$ mm and three hundred times bigger than the true modulus gradient $W_T = 50$ μm. True modulus transition width can be seen from microscopic imaging of the diffusion of coloration between the two gels and is 50 μm. Simulation of the indentation mapping experiment with stiff and compliant side elastic moduli of $E_S = 0.23$ MPa and $E_C = 0.06$ MPa respectively, contact diameter and true modulus transition of $d = 5.3$ mm and $W_T = 50$μm. The model accurately predicted both the shape of $E_O(x)$ and the observed width of the transition W_O to be 14.2 mm.

During indentation the interface was imaged from below to observe how the interface deformed, Fig. 8 shows the stiff gel bowing out into the compliant gel. The observed bowing can be understood by considering the limiting case, indenting in a line from a stiff material toward the interface with the compliant material is similar to indenting at the edge of that stiff material in free space.

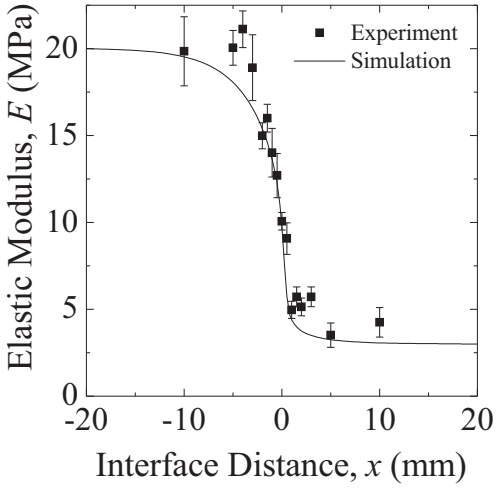

Fig. 6. Plot of elastic modulus vs distance from the interface, comparing the simulated observed modulus function and the experimental observed modulus function for a PDMS-nickel composite. Simulation indentation parameters were matched to those of the experiment, elastic moduli of $E_S = 19$ MPa and $E_C = 3$ MPa were used with the width of the simulated transition region being $W_T = 250$ μm.

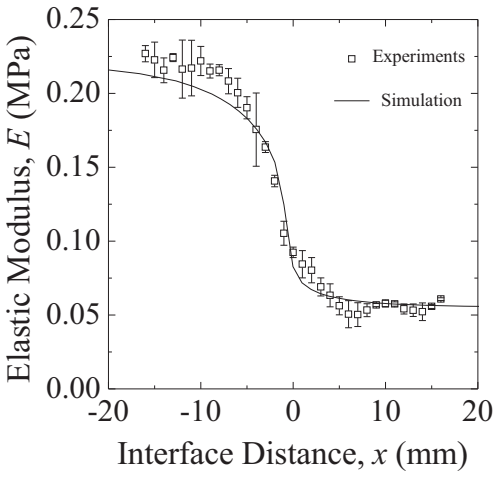

Fig. 7. Plot of elastic modulus vs distance from the interface, comparing the simulated observed modulus function and the experimental observed modulus function for an interface between a 7.5% and 20% gelatin gel. Simulation indentation parameters were matched to those of the experiment, elastic moduli of $E_S = 0.23$ MPa and $E_C = 0.06$ MPa with the transition region being $W_T = 50$ μm wide.

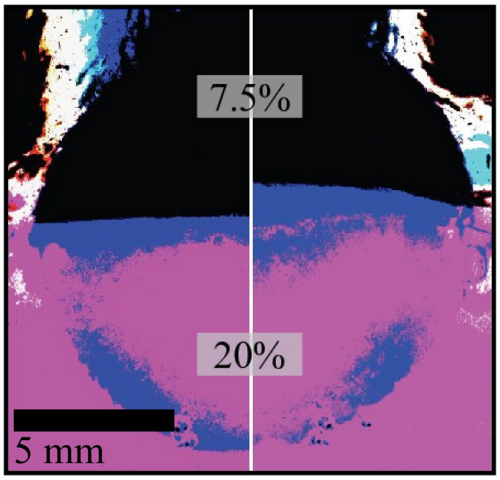

Fig. 8. High contrast images showing the interface between 7.5 wt% and 20 wt% gelatin gels during indentation. Left, slight bowing of the interface at the start of the indent, 1 % characteristic strain. Right, significant bowing of the interface at the maximum indentation depth, 11 % characteristic strain.

The sample can bulge outwards into the compliant material to accommodate load, lowering the apparent stiffness near the edge. Conversely, indenting from a compliant material towards an interface with a stiff material is similar to indenting at the edge of a compliant material constrained by a wall at its edge and hence the apparent stiffness close to the edge is increased. Both of these effects can be simultaneously observed in the deformation of the interface boundary imaged in the gelatin sample shown in Fig. 8.

3.2.3. Partially demineralized bone

The observed gradient in modulus for this sample is $W_O = 3.2$ mm (Fig. 9), three times greater than the contact diameter of the indent, $d = 0.9$ mm and three hundred times bigger than the true modulus gradient $W_T = 200$ μm. For these samples the true width of the interface is in the range 100–300 μm from observation under an optical microscope of demineralization. For the simulation of this experiment, the transition was modeled as 200 μm wide. Simulation of the indentation mapping experiment with stiff and compliant side elastic moduli of $E_S = 97.2$ MPa and

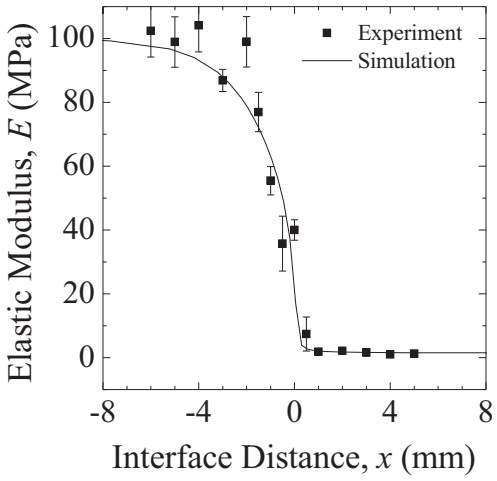

Fig. 9. Plot of modulus vs distance from the interface, comparing the simulated observed modulus function and the experimental observed modulus function for an interface between mineralised and demineralised porcine scapula. Simulation indentation parameters were matched to those of the experiment and sample with elastic moduli of $E_S = 97.2$ MPa and $E_C = 1.56$ MPa and $W_T = 200\mu$m wide.

$E_C = 1.56$ MPa respectively, contact diameter and true modulus transition of $d = 0.9$ mm and $W_T = 200$ μm. The model accurately predicted both the shape of $E_O(x)$ and the observed width of the transition W_O to be 3.4 mm. Indentation across the partially demineralized bone showed that the elastic modulus varied from 97.2–1.6 MPa from the mineralized to the demineralized bone. The mineralized bone in this experiment is porous cancellous bone and hence it is unsurprising that the modulus measured with a large indenter tip *i.e.* the bulk foam response, is smaller than the GPa range normally reported for cortical bone or single wall tests of cortical bone.

3.2.4. Literature indentation mapping

From literature there are two examples of indentation line mapping of stiff-compliant tissue interfaces under hydrated, elastic conditions [33,34]. Both of these papers study the meniscal insertion site and the relevant modulus functions from each have been reproduced in Fig. 10. The material and indentation experimental conditions of these literature examples were recreated in the model with an assumption that the true modulus gradient was 30μm as found by dehydrated indentation of the same tissue by [30]. From the experimental conditions alone, the model accurately predicted that the 95% width of the observed modulus interface would be $W_O = 250$ μm, the model predictions can also be seen in Fig. 10.

4. Discussion

Gradients are ubiquitous in biological materials, and fulfill important material functions. However, an accurate quantification of such small-scale variations in material properties via instrumented indentation is often difficult, due to the competition between two inherent length scales, the diameter, d, of the contact area, and the width, W, of the transition in elastic properties. This work uses both experiments and finite element simulations to investigate the use of indentation to determine the mechanical properties of interface tissues such as bone–tendon, bone–ligament and bone–cartilage. These results clearly show that features within the observed modulus function, $E_O(x)$, appear wider than in the true function of modulus of the sample, $E_T(x)$. This effect can be seen in the simulations herein, Figs. 3 and 4, show that if the contact diameter is comparable to or larger than the modulus

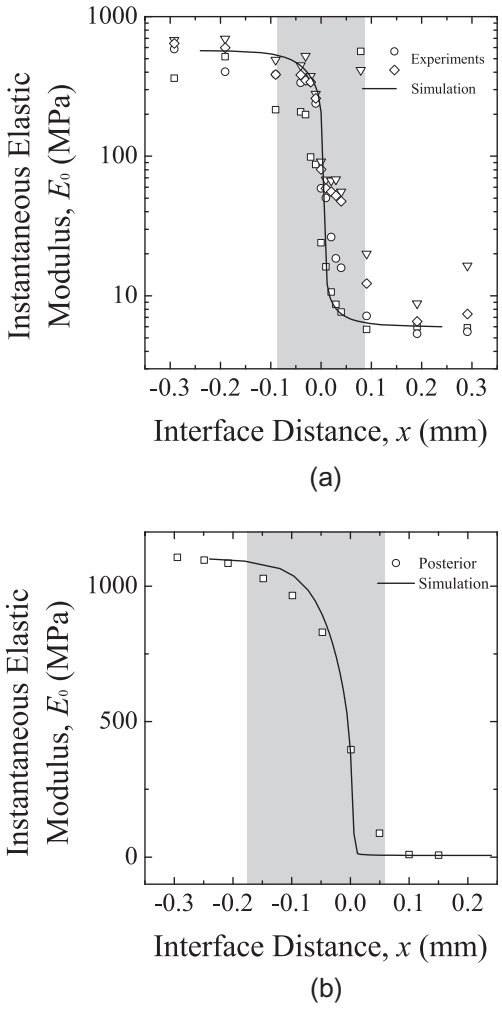

Fig. 10. Plots of the elastic modulus vs distance from the interface, showing the experimental observed modulus function from a) Abraham [33] and b) Hauch [34], plotted alongside simulations of the observed modulus function conducted by this author. Simulations of their experiments used indentation parameters taken from the respective papers and a true interface width of $W_T = 30$ μm. Plots have been reproduced for comparison from the original papers by digitizing the data.

features within the sample, that the observed modulus function is more dependent on the indenter to feature size ratio, than on the sample parameters an investigator seeks to elucidate. This effect is also observed in a variety of experimental samples that validate the model to show that the observed modulus function, $E_O(x)$, of a sample when tested under specific conditions can be predicted with simulations, Figs. 6, 7, 9 and 10. It can be seen that for the parameters of the samples included herein (typical of bone–tendon or bone–cartilage interfaces) the width of the observed function is consistently just over three times the diameter of the contact patch between indenter and sample.

The literature examples of indentation line mapping of stiff-compliant tissue interfaces under hydrated, elastic conditions [33,34] are also used to further validate the model. Both of these papers study the meniscal insertion site. In both papers the 95% width of the modulus interface observed through indentation is found to be approximately $W_O = 250$ μm. Similar to the size of the total structural change in the enthesis that can be observed through histology through subchondral bone, calcified fibrocartilage, uncalcified fibrocartilage and ligament proper [38,39]. Yet, in a different study when analyzing the dehydrated interface of patellae cartilage, through both indentation and qBSE, find the change in modulus to occur primarily at the mineralization tide-

mark and be around 30 μm wide [30]. Further work [40] on the mineral distribution of the bone–tendon insertion suggests that while the mineral content may vary over a 120 μm distance, the mechanical transition occurs over a shorter length scale than this that represents the position in the interface where the mineral concentration goes above a certain percolation threshold to form a connected network. Additionally, while there are a lack of direct mechanical studies on other similar ligamentous type insertions, many studies have chemically observed the change in mineral content to be on the order of 10 μm [14,19]. The observed effect in [33,34] is therefore shown to be unsurprising as both studies conducted indentation with contact diameters in the range 10–20 μm, similar to the 30 μm wide modulus interface suggested by other authors. Hence, their modulus functions appear wider than it truly is within the material and this is predicted with the model.

During elastic spherical indentation [41] a strain field is generated under the indenter that is much larger than the contact diameter of the indent. The modulus calculated by Hertzian contact is based on the reaction load on the indenter tip. This load can be considered as the sum of the 3D compressive reactions of each element of material within the strain field of the indenter, where the compressive reaction from any single element is dependent on its stiffness. In this way it can be seen that the indenter is detecting load by a non-uniform summation of a volume around and underneath the contact patch. Ordinarily in homogeneous materials—or in cases where the indentation contact diameter is very small compared to the features being examined—the stiffness of each theoretical element that undergoes strain is the same and hence an accurate elastic modulus for that region of material is obtained. However, when the contact diameter (and hence the strain field) are large compared to the modulus features in question then a single indent samples the entire interface region of the sample where each element can have vastly different stiffnesses, Fig. 11. This means that when indents are a similar size to the interface a blurring or widening of modulus features is observed. This implications of this have been considered by Randall for a particle composite material, where a nondimensional size h/D is defined where h is the indentation depth and D is the size of composite phase[27]. Randall states that if $h/D \ll 1$ then measured properties are characteristic of the phase of size D, if $h/D \gg 1$ then measured properties are characteristics of the whole composite material. Hence this effect has been considered as a possibility but has not, until now, been analyzed for mechanical investigation of interface tissues, for which indentation is often considered an attractive option.

This work focuses on indentation with spherical indenter tips that stays in an elastic regime *i.e.* characteristic strain <5%, Eq. (2). While it is similarly true for higher strain spherical indents, or indents with sharp tips that transition into plastic deformation of the sample, that the strain field under the indenter is larger than the contact patch and hence a similar blurring would be observed, the exact limits at which this occurs are not discussed herein. Further, this work makes use of a purely elastic model of the materials being tested which is not truly representative of natural bone or soft tissues which both exhibit time dependency in the form of significant poroelasticity and viscoelasticity [31,32,42]. The lack of poroelastic or viscoelastic considerations in this work does not limit its applicability as the equilibrium time measurements of time dependent materials will likewise be subject to these effects. However the investigation of mapping elastic modulus transitions in time dependent materials should be the subject of future work. Additionally, many natural tissues, especially ligament and tendon that are the subject of this discussion, are highly anisotropic which is not accounted for in this model. Because indentation gives rise to a 3D stress field it samples all axes of the sample. Hence modulus measured by indentation is some complex combination of the moduli in the three independent axes. As such the degree of anisotropy of a material is less apparent in the indentation modulus than had the sample been tested in each dimension independently [43]. Regardless of anisotropy the problem with indenting across gradients is that the stress field is large compared to the inhomogeneity of the material in question. While anisotropy certainly causes the stress field to change shape it does not diminish the central point that the stress field is large and hence blurring of apparent width occurs. This dose not reduce the validity of the model but means that the representative indentation modulus is different to the moduli of any of the independent axes and should be modeled as such. Finally, it should be noted that elastic modulus as determined through indentation is likely to be smaller than that observed through tensile or bulk compression testing, especially for soft tissues [44]. However indentation allows testing of local tissue variations that can not be isolated by a bulk tensile or compressive experiment and hence provides significant valuable information, assuming the data is analyzed in the context of qualitative variations rather than absolute values.

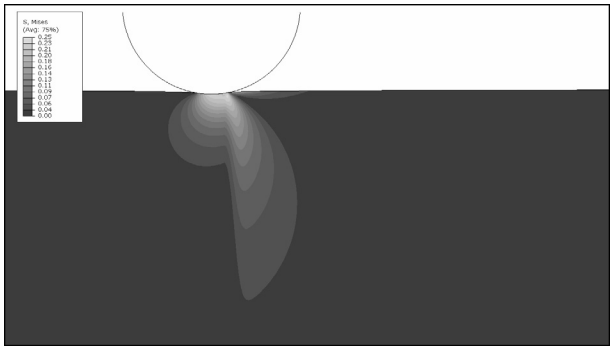

Fig. 11. A von Mises stress contour plot of indentation over an interface between a stiff material (right) and compliant material (left). The transition region is centered at the right-hand edge of the contact patch.

At the time of writing, current nanoindentation techniques are not sufficiently sensitive to allow for the contact diameter of the indent to be considerably smaller than the mechanical gradients that occur naturally in tissue interfaces in the range 10–50 μm [29]. A typical commercial nanoindenter has a load range of approximately 1 μN to 10 mN. On a hydrated soft tissue with moduli typically of the order 10–100 MPa the smallest contact diameter of indents possible (Eq. 1) with an appropriate sized tip, 250–500 μm, is approximately 30 μm which is of the same order in size as the interface in natural tissues. This is the case for the enthesis of the bone–tendon junction or the osteochondral interface where the interface width, as determined by chemical variations, is on the order of 10 μm to30 μm [19,30,45], while the required indenter parameters for hydrated materials using a commercial nanoindenter often result in a 20 μm diameter contact patch. Thus, samples should either be tested dehydrated to allow smaller indents with commercial nanoindenters with the acceptance that the material parameters will only be qualitatively useful. Or if testing hydrated then colloidal probe AFM indentation with smaller measurable loads and hence smaller contact diameters could be used.

5. Conclusions

When conducting indentation of biological stiff-compliant tissue interfaces care must be taken over the size of the contact patch relative to the material features being examined. Two distinct cases arise from this work and the rule of thumb for indentation of interfaces between stiff and compliant tissues for spherical indentation is as follows: firstly, if the length scale of indentation is distinctly smaller than the modulus gradients within the sample,

$d/W \leqslant 0.1$, instrumented indentation can accurately map mechanical properties; secondly, if the length scale of indentation is equal to or greater than the elastic modulus gradients in the sample, $d/W \geqslant 1$, then the observed modulus function is more dependent on the indenter to feature size ratio, d/W, than on the sample and W_O will appear approximately three times the size of the contact patch, d, regardless of true material properties. Assuming the limit of elastic strain, <5%, this gives a suggested indenter radius, $R \leq 1.6 \times W_T$, where the best guess for W_T, the expected feature size of a transition in modulus, must be made in advance to assess the likely applicability of instrumented indentation. It should be noted that in the extreme case, a infinitely sharp transition from stiff to compliant, a gradient will always be observed with any sized indenter tip and that this gradient will appear smaller with smaller indenter tips. This also implies that data collected with a too large tip can not be worked backwards to infer the true modulus map as it is more dependent on d than on W_T. Ideally the contact patch of the indent should be one order of magnitude smaller than the size of the modulus features to be investigated.

5.1. Acknowledgements:

This work was supported by the UK Engineering and Physical Sciences Research Council (EPSRC) via the Doctoral Training Award, Department of Engineering, University of Cambridge, Grant No. 1220717. Supporting research data as required by EPSRC research policy may be accessed at {https://doi.org/10.17863/CAM.6491}. The authors would like to acknowledge Manon VanThorenburg for preparation and characterization of gelatin gels and are grateful to Dr. David Labonte for helpful discussions while preparing the manuscript.

References

[1] K. Yamaguchi, New guideline on rotator cuff problems, American Academy of Orthopaedic Surgeons, 2011. Technical Report.
[2] K. Miyasaka, D. Daniel, M. Stone, P. Hirshman, The incidence of knee ligament injuries in the general population, Am. J. Knee Surg. 4 (1991) 3–8.
[3] OECD, Hip and Knee Replacement, in: Heal. a glance 2013 OECD Indic., OECD Publishing, 2013.
[4] P. Bernstein, M. Bornhäuser, K. Günther, M. Stiehler, Bone tissue engineering in clinical application: assessment of the current situation, Orthopade 38 (2009) 1029–1037.
[5] P.B. Voleti, M.R. Buckley, L.J. Soslowsky, Tendon healing: repair and regeneration, Ann. Rev. Biomed. Eng. 14 (2012) 47–71.
[6] J. Jiang, A. Tang, G.A. Ateshian, X. Edward Guo, C.T. Hung, H.H. Lu, Bioactive stratified polymer ceramic- hydrogel scaffold for integrative osteochondral repair, Ann. Biomed. Eng. 38 (2010) 2183–2196.
[7] A.K. Lynn, S.M. Best, R.E. Cameron, B.A. Harley, I.V. Yannas, L.J. Gibson, W. Bonfield, Design of a multiphase osteochondral scaffold. I. Control of chemical composition, J. Biomed. Mater. Res. – Part A 92 (2010) 1057–1065.
[8] B.A. Harley, A.K. Lynn, Z. Wissner- Gross, W. Bonfield, I.V. Yannas, L.J. Gibson, Design of a multiphase osteochondral scaffold. II. Fabrication of a mineralized collagen-glycosaminoglycan scaffold, J. Biomed. Mater. Res. – Part A 92 (2010) 1066–1077.
[9] B.A. Harley, A.K. Lynn, Z. Wissner- Gross, W. Bonfield, I.V. Yannas, L.J. Gibson, Design of a multiphase osteochondral scaffold III: Fabrication of layered scaffolds with continuous interfaces, J. Biomed. Mater. Res. – Part A 92 (2010) 1078–1093.
[10] S.R. Caliari, M.A. Ramirez, B.A.C. Harley, The development of collagen-GAG scaffold-membrane composites for tendon tissue engineering, Biomaterials 32 (2011) 8990–8998.
[11] J.P. Spalazzi, E. Dagher, S.B. Doty, X.E. Guo, S.A. Rodeo, H.H. Lu, In vivo evaluation of a multiphased scaffold designed for orthopaedic interface tissue engineering and soft tissue-to-bone integration, J. Biomed. Mater. Res. Part A 86 (2008) 1–12.
[12] H.H. Lu, S.D. Subramony, M.K. Boushell, X. Zhang, Tissue engineering strategies for the regeneration of orthopedic interfaces, Ann. Biomed. Eng. 38 (2010) 2142–2154.
[13] S.A. Rodeo, S.P. Arnoczky, P.A. Torzilli, C. Hidaka, R.F. Warren, Tendon-healing in a bone tunnel. A biomechanical and histological study in the dog, J. Bone Jt. Surg. 75 (1993) 1795–1803.
[14] H.H. Lu, S. Thomopoulos, Functional attachment of soft tissues to bone: development, healing, and tissue engineering, Ann. Rev. Biomed. Eng. 15 (2013) 201–226.
[15] X. Li, J. Xie, J. Lipner, X. Yuan, S. Thomopoulos, Y. Xia, Nanofiber scaffolds with gradations in mineral content for mimicking the tendon-to-bone insertion site, Nano Lett. 9 (2009) 2763–2768.
[16] H.W. Cheng, K.D.K. Luk, K.M.C. Cheung, B.P. Chan, In vitro generation of an osteochondral interface from mesenchymal stem cell- collagen microspheres, Biomaterials 32 (2011) 1526–1535.
[17] N.T. Khanarian, J. Jiang, L.Q. Wan, V.C. Mow, H.H. Lu, A hydrogel-mineral composite scaffold for osteochondral interface tissue engineering, Tissue Eng. Part A 18 (2012) 533–545.
[18] K.L. Moffat, W.H.S. Sun, N.O. Chahine, P.E. Pena, S.B. Doty, C.T. Hung, G.A. Ateshian, H.H. Lu, Characterization of the mechanical properties and mineral distribution of the anterior cruciate ligament-to-bone insertion site, Conf. Proc. IEEE Eng. Med. Biol. Soc. (2006) 2366–2369.
[19] K.L. Moffat, W.-H.S. Sun, P.E. Pena, N.O. Chahine, S.B. Doty, G.A. Ateshian, C.T. Hung, H.H. Lu, Characterization of the structure-function relationship at the ligament-to- bone interface, Proc. Natl. Acad. Sci. U.S.A. 105 (2008) 7947–7952.
[20] A.J. Engler, S. Sen, H.L. Sweeney, D.E. Discher, Matrix elasticity directs stem cell lineage specification, Cell 126 (2006) 677–689.
[21] T. Lü hmann, H. Hall, Cell guidance by 3D-gradients in hydrogel matrices: importance for biomedical applications, Materials (Basel) 2 (2009) 1058–1083.
[22] G.M. Pharr, Measurement of mechanical properties by ultra-low load indentation, Mater. Sci. Eng. A 253 (1998) 151–159.
[23] J.L. Cuy, A.B. Mann, K.J. Livi, M.F. Teaford, T.P. Weihs, Nanoindentation mapping of the mechanical properties of human molar tooth enamel, Arch. Oral Biol. 47 (2002) 281–291.
[24] A. Miserez, T. Schneberk, C. Sun, F.W. Zok, J.H. Waite, The transition from stiff to compliant materials in squid beaks, Science 319 (2008) 1816–1819.
[25] H. Peisker, J. Michels, S.N. Gorb, Evidence for a material gradient in the adhesive tarsal setae of the ladybird beetle Coccinella septempunctata, Nat. Commun. 4 (2013) 1661.
[26] G. Constantinides, K.S. Ravi Chandran, F.J. Ulm, K.J. Van Vliet, Grid indentation analysis of composite microstructure and mechanics: principles and validation, Mater. Sci. Eng. A 430 (2006) 189–202.
[27] N.X. Randall, M. Vandamme, F. Ulm, Nanoindentation analysis as a two-dimensional tool for mapping the mechanical properties of complex surfaces, J. Mater. Res. 24 (2009) 679–690.
[28] A. Dwivedi, T.J. Wyrobek, O.L. Warren, J. Hattrick- Simpers, O.O. Famodu, I. Takeuchi, High-throughput screening of shape memory alloy thin-film spreads using nanoindentation, J. Appl. Phys. 104 (2008) 073501.
[29] M.L. Oyen, Handbook of Nanoindentation: With Biological Applications, Pan Stanford Press/ World Scientific Publishing, Singapore, 2011.
[30] H.S. Gupta, S. Schratter, W. Tesch, P. Roschger, A. Berzlanovich, T. Schoeberl, K. Klaushofer, P. Fratzl, Two different correlations between nanoindentation modulus and mineral content in the bone-cartilage interface, J. Struct. Biol. 149 (2005) 138–148.
[31] A. Bembey, A. Bushby, A. Boyde, V.L. Ferguson, M. Oyen, Hydration effects on the micro-mechanical properties of bone, J. Mater. Res. 21 (2006) 1962–1968.
[32] A. Bembey, M. Oyen, A. Bushby, A. Boyde, Viscoelastic properties of bone as a function of hydration state determined by nanoindentation, Philos. Mag. 86 (2006) 5691–5703.
[33] A.C. Abraham, T.L. Haut Donahue, From meniscus to bone: a quantitative evaluation of structure and function of the human meniscal attachments, Acta Biomater. 9 (2013) 6322–6329.
[34] K.N. Hauch, M.L. Oyen, G.M. Odegard, T.L. Haut Donahue, Nanoindentation of the insertional zones of human meniscal attachments into underlying bone, J. Mech. Behav. Biomed. Mater. 2 (2009) 339–347.
[35] D. Tabor, The Hardness of Metals, Clarendon Press, London, 1951.
[36] R. Shahar, P. Zaslansky, M. Barak, A.A. Friesem, J.D. Currey, S. Weiner, Anisotropic Poisson's ratio and compression modulus of cortical bone determined by speckle interferometry, J. Biomech. 40 (2007) 252–264.
[37] H. Jin, J.L. Lewis, Determination of Poisson's ratio of articular cartilage by indentation using different-sized indenters, J. Biomech. Eng. 126 (2004) 138–145.
[38] H. Yahia, N. Newman, Tendon and ligament insertion. A light and electron microscopic study, J. Bone Jt. Surg. 52 (1970) 664–674.
[39] M. Benjamin, E.J. Evans, L. Copp, The histology of tendon attachments to bone in man, J. Anat. 149 (1986) 89–100.
[40] G.M. Genin, A. Kent, V. Birman, B. Wopenka, J.D. Pasteris, P.J. Marquez, S. Thomopoulos, Functional grading of mineral and collagen in the attachment of tendon to bone, Biophys. J. 97 (2009) 976–985.
[41] K. Johnson, Contact Mechanics, Cambridge University Press, 1985.
[42] M.L. Oyen, T.A. Shean, D.G. Strange, M. Galli, Size effects in indentation of hydrated biological tissues, J. Mater. Res. 27 (2012) 245–255.
[43] J.G. Swadener, J.Y. Rho, G.M. Pharr, Effect of anisotropy on elastic moduli measured by nanoindentation in human tibial cortical bone, J. Biomed. Mater. Res. 57 (2001) 108–112.
[44] C.T. McKee, J.A. Last, P. Russell, C.J. Murphy, Indentation versus tensile measurements of Young's modulus for soft biological tissues, Tissue Eng. Part B Rev. 17 (2011) 155–164.
[45] J.P. Spalazzi, A.L. Boskey, H.H. Lu, Region-dependent variations in matrix collagen and mineral distribution across the femoral and tibial anterior cruciate ligament-to-bone insertion sites, in: 53rd Annu. Meet. Orthop. Res. Soc., 2007.